ACS APPLIED MATERIALS & INTERFACES

Research Article

Cite This: ACS Appl. Mater. Interfaces 2019, 11, 32879−32886

www.acsami.org

# Electrodeposition of $MoS_x$ Hydrogen Evolution Catalysts from Sulfur-Rich Precursors

Oluwaniyi Mabayoje,[†] Yang Liu,[‡,§] Michael Wang,[‡] Ahmed Shoola,[†] Amani M. Ebrahim,[∥] Anatoly I. Frenkel,[∥,⊥] and C. Buddie Mullins*[,†,‡,#]

[†]Department of Chemistry, [‡]Department of Chemical Engineering, and [#]Texas Materials Institute, University of Texas at Austin, Austin, Texas 78712, United States

[§]College of Chemistry and Chemical Engineering, Central South University, Changsha 410083, China

[∥]Department of Materials Science and Chemical Engineering, Stony Brook University, Stony Brook 11794, United States

[⊥]Chemistry Department, Brookhaven National Laboratory, Upton, New York 11973, United States

Supporting Information

**ABSTRACT:** Amorphous molybdenum sulfides (a-$MoS_x$) are known to be active electrocatalysts for the hydrogen evolution reaction (HER), but the role stoichiometry of the sulfur atoms plays in the HER activity remains unclear. In this work, we deposited thin films of a-$MoS_x$ from two thiomolybdate deposition baths with different sulfur ratios ($MoS_4^{2-}$ and $Mo_2S_{12}^{2-}$) and showed that the sulfur stoichiometry, as determined by X-ray photoelectron spectroscopy, is controlled by the precursor of choice and the electrochemical method used to deposit the thin films. Using the $Mo_2S_{12}^{2-}$ precursor allows access to a $MoS_6$ thin film, with a higher S/Mo ratio compared with that of any previously reported electrodeposited films. We also examined the effect of electrochemistry on the resulting S/Mo ratio in the as-prepared a-$MoS_x$ thin films. Samples with S/Mo ratios ranging from 2 to 6 were electrodeposited on glassy carbon (GC) substrates by using anodic, cathodic, or cyclic voltammetry deposition. The a-$MoS_x$ thin films deposited on GC substrates were tested as HER catalysts in acidic electrolytes. The overpotentials needed to drive current densities of 10 mA/cm$^2$ ranged from 160 mV for $MoS_6$ samples to 216 mV for $MoS_2$ samples, signifying the important role sulfur content plays in HER activity of the prepared films. Furthermore, we characterized the deactivation of the a-$MoS_x$ films and found that the sulfur content is gradually depleted over time, leading to a slow deactivation of the a-$MoS_x$ thin-film catalysts. We showed a facile procedure that affords a-$MoS_x$ films with high sulfur content by using S-rich precursors and highlighted the role of sulfur in the prepared films for HER.

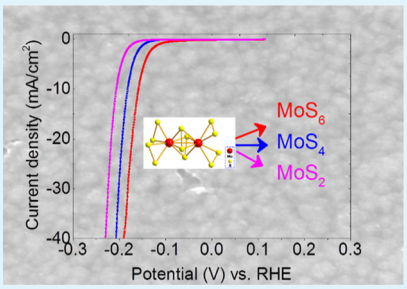


**KEYWORDS:** *hydrogen evolution, electrocatalysis, molybdenum sulfide, thin films, energy conversion, solar water splitting*

## 1. INTRODUCTION

Photoelectrochemical (PEC) water splitting or photovoltaic electrolysis is a process in which the energy from sunlight is used to produce hydrogen ($H_2$) and oxygen ($O_2$) from water ($H_2O$). The conversion of an intermittent source of energy such as solar energy into a storable chemical fuel such as $H_2$ can help in ameliorating global energy problems and the world's reliance on fossil fuels.[1−3] The hydrogen evolution reaction (HER) is one of the two reactions involved in water splitting. It is also an example of an inner-sphere electrochemical reaction where the reactant, intermediates, and products are specifically adsorbed on the electrocatalyst surface.[4] For this reason, electrocatalysts are important, and the scientific community is focused on studying and finding economical transitional-metal catalysts that are active and stable for the HER.[5−7]

Inspired by nitrogenase enzymes, which contain clusters of iron sulfides and a molybdenum cofactor responsible for the reduction of nitrogen to ammonia in biological systems, researchers discovered that crystalline molybdenum sulfide ($MoS_2$) with structural and "active sites" similar to this enzyme can be used as a proton-reducing catalyst.[8] This catalyst, however, is typically prepared at high temperatures and requires a preferential exposure or high density of $MoS_2$ edge sites to act as an active catalyst for the HER.[9−11] Hu et al. showed that amorphous molybdenum sulfide (a-$MoS_x$) materials prepared at low temperatures either as particles or as thin films by electrochemical deposition from a $MoS_4^{2-}$ solution using cyclic voltammetry (CV), anodic, or cathodic currents can be used as HER catalysts.[12−14] These a-$MoS_x$ materials readily outperform their crystalline counterparts and can be used directly as electrodes or coated on photocathodes/photocatalysts for PEC water splitting.[15−17] The possibility of fine-tuning the properties of the materials by synthetic methods and electrode preparation makes electrodeposited films desirable as a means to improve the performance of thin

Received: April 25, 2019
Accepted: August 15, 2019
Published: August 15, 2019






DOI: 10.1021/acsami.9b07277
ACS Appl. Mater. Interfaces 2019, 11, 32879−32886

films for HER catalyst applications. Furthermore, these a-$MoS_x$ thin films can be used in other electrochemical applications such as batteries.[18−20]

Recent research has indicated that a-$MoS_x$ materials are inorganic polymers of molybdenum and sulfur clusters.[18,21,22] Tran and co-workers resolved the Mo/S clusters in a-$MoS_x$ by transmission electron microscopy (TEM) imaging, which were shown as chains of $Mo_3S_{13}$ units in the a-$MoS_x$ polymer.[21,23,24] Another interesting aspect of electrodeposited a-$MoS_x$ films is the possibility of controlling the stoichiometry of the thin films using electrochemistry.[12,25] Hu et al. showed that cathodic deposition (CD) resulted in the formation of $MoS_2$ films while anodic deposits led to the formation of $MoS_{3.6}$ films, whereas films deposited using CV gave a 3:1 sulfur-to-molybdenum ratio, presumably being a mixture of the anodic and cathodic products.[12] The relative amounts of S and Mo in anodic ($MoS_3$) and cathodic ($MoS_2$) a-$MoS_x$ catalysts were shown to influence the type of sulfur moieties present in the material as indicated by the ratio of higher binding sulfur peaks in the S 2p region in X-ray photoelectron spectroscopy (XPS) measurements. Ting and co-workers showed that anodic $MoS_3$ films had a higher ratio of the $S_{HBE}$-active sites for the HER compared to cathodic $MoS_2$ films.[25,26] However, the effect of an increase in the amount of sulfur in the films on the HER activity of these catalysts has not been explored.

In this work, taking advantage of the rich chemistry of thiomolybdates, we show that it is also possible to control the stoichiometry and increase the S/Mo ratio of a-$MoS_x$ thin-film catalysts by using a $Mo_2S_{12}^{2-}$ precursor. Thiomolybdates have been previously explored either in fundamental studies focused on bonding and structures of these inorganic compounds (especially for their structural similarities to nitrogenase enzymes) or in the application of these materials as classical hydrodesulfurization catalysts.[27,28] Although researchers have shown that it is possible to modify the structure and activity of a-$MoS_x$ HER catalysts by changing the method of deposition (anodic vs cathodic), exploring the effects of utilizing other thiomolybdate precursors in thin-film preparation has not been addressed. Furthermore, the catalytic performance when the sulfur content is further increased in the a-$MoS_x$ prepared thin films remains an important parameter to correlate structure−property relationships in HER-based catalysis.

Here, we study the physical and chemical properties of these films focusing on the electrochemical evolution of hydrogen. Thin films with a range of stoichiometries were synthesized and characterized using spectroscopic methods. We successfully prepared thin-film catalysts with a S/Mo ratio as high as 6 from this thiomolybdate precursor. The films were characterized using complimentary techniques, which showed the uniformity of deposition and thickness of the films. Raman spectroscopy also shows the typical two bands inherent to the thin a-$MoS_x$ film with the S/S and Mo/S vibrational modes. XPS results show that the ratio of bridging and terminal sulfur groups in the thin films is dependent on the precursor used and the electrochemical procedure used for the deposition. Extended X-ray absorption fine structure (EXAFS) analysis provides evidence of the effect of precursor choice on the coordination environment around Mo. The thin films were tested as HER catalysts, and it was determined that the sulfur content of a-$MoS_x$ films influenced their performance as electrocatalysts with the highest S/Mo ratios showing the highest activity (lowest overpotential) for the HER. These $MoS_6$ thin films have one of the highest known ratios for S/Mo reported in the literature for a-$MoS_x$ materials. The observation that sulfur content in the precursor influences the stoichiometry of metal sulfide films also means that the sulfur-to-molybdenum ratios as high as 9 could likely be achieved by electrodepositing using $MoS_9^{2-}$ as a precursor.[27]

## 2. EXPERIMENTAL SECTION

**2.1. Materials.** Ammonium molybdate tetrahydrate [$(NH_4)_6Mo_7O_{24}{\cdot}4H_2O$ 81.0−83.0% $MoO_3$ basis], carbon disulfide ($CS_2$ 99+%), and diethyl ether ($C_4H_{10}O$ 98%) were purchased from Sigma-Aldrich. Hydroxylamine hydrochloride ($NH_2OH{\cdot}HCl$ 99+%) was purchased from Acros Organics. Ammonium sulfide ($NH_4S_x$ 20−24% aqueous solution) was purchased from Alfa Aesar. Sulfuric acid (0.5 M, $H_2SO_4$, ACS certified), sulfur, potassium monobasic phosphate, and potassium dibasic phosphate were purchased from Fisher Scientific. All chemicals were used as received. Milli-Q water (>18 MΩ cm resistivity) was used in preparing all solutions.

**2.2. Ammonium Tetrathiomolybdate Synthesis.** $(NH_4)_2MoS_4$ was made by mixing 1.5 g of ammonium molybdate tetrahydrate with 20 mL of ammonium sulfide (20−24%) at 50 °C for 30 min and then cooling in an ice bath for 4 h. Red crystals with a green shimmer formed from this reaction were filtered, washed with 10 mL of isopropanol and 10 mL of ice-cold water, and then dried in argon for 24 h.

**2.3. Ammonium Thiodimolybdate Synthesis.** $(NH_4)_2Mo_2S_{12}$ was made following the methods previously described by Huang et al.[29] Briefly, we mixed 30 mL of ammonium sulfide with 7.1 g of sulfur powder and stirred this mixture at 50 °C for 15 min or until all the sulfur dissolved in the orange ammonium sulfide solution to give a red solution. This solution was then mixed with 30 mL of a solution containing 2 g of ammonium molybdate tetrahydrate and 1.5 g of hydroxylamine hydrochloride and allowed to stir at 50 °C for 2 h. This solution is filtered, and the filtrate is stirred at 90 °C for another 4 h. After 4 h, the solution is cooled to room temperature, mixed with 20 mL of ammonium sulfide, and allowed to stand overnight (∼12 h) in an argon atmosphere. Black crystals formed in the solution overnight which were filtered and sequentially washed with 10 mL of ice-cold water, 10 mL of ice-cold ethanol, 10 mL of carbon disulfide, and 20 mL of diethyl ether, and then dried and stored in an argon atmosphere.

**2.4. Film Deposition.** Fluorine-doped $SnO_2$ (FTO) glass substrates were cleaned by sonication in a 1:1 mixture of Contrex and ethanol, water, acetone, and finally water for 10 min each and then dried in a vacuum furnace for 30 min at 100 °C. An area of ∼1 $cm^2$ was masked off the precleaned 2 × 1 cm square FTO glass using a 3M 470 electroplating tape. A glassy carbon (GC) (3 mm diameter) disk electrode substrate was polished with alumina powders and then briefly sonicated in a 1:1 solution of ethanol and water to remove alumina particles. Silver/silver chloride (Ag/AgCl) (saturated potassium chloride, KCl) and a graphite rod were used as the reference and counter electrodes (CEs), respectively.

*2.4.1. $Mo_2S_{12}^{2-}$-Based Films.* The electrodeposition bath was made of 1 mM $Mo_2S_{12}^{2-}$ (2 mM Mo) and 0.1 M phosphate buffer solution at pH 7. Anodic deposition (AD) was achieved by applying a potential of −0.1 V versus Ag/AgCl leading to the deposition of uniform brown films on FTO substrates. A potential of −0.9 V versus Ag/AgCl was applied to deposit films by cathodic deposition (CD). Potential cycling deposition scans were carried out between 0.1 and −1 V (CV). The films were rinsed in Milli-Q water and dried in an argon stream.

*2.4.2. $MoS_4$ (AD) Deposition (from $MoS_4^{2-}$).* The electrodeposition bath was made of 2 mM $MoS_4^{2-}$ and 0.1 M phosphate buffer solution. A potential of 0.3 V versus Ag/AgCl was applied for 300 s, leading to the deposition of visually uniform films. The films were similarly rinsed in Milli-Q water and dried in an argon stream.

**2.5. Electrochemical Characterization.** All potentials were recorded against a Ag/AgCl (saturated KCl) reference electrode with Teflon frits from CH Instruments and reported against the reversible hydrogen electrode (RHE), except where otherwise noted. A carbon


DOI: 10.1021/acsami.9b07277
ACS Appl. Mater. Interfaces 2019, 11, 32879−32886

rod was used as the CE. We estimated the HER activity of films using CV. First, we carried out 20 CV scans between 0.2 and −0.4 V versus RHE at a scan rate of 100 mV/s and a resistance-corrected linear sweep voltammetry scan at a scan rate of 10 mV/s between 0.2 and −0.25 V versus RHE was recorded for all samples.

**2.6. Physical Characterization.** A Quanta FEG scanning electron microscope equipped with a Bruker XFlash 5010 detector was used for imaging and a Hitachi SS5500 was used for cross-sectional SEM. X-ray diffraction patterns were acquired with an ULTIMA diffractometer with a Cu K$\alpha$ radiation source. Raman spectroscopy was performed with a WiTec alpha300 confocal microscope system with a 488 nm wavelength and 1 mW laser power at 100× objective. Atomic force microscopy (AFM) measurements were made using a Park Scientific XE-100. A Kratos Axis Ultra spectrometer with a monochromated Al K$\alpha$ source was used to take XPS data, which were used in measuring the stoichiometry and chemical states of species in the a-$MoS_x$ films. EXAFS measurements were performed at the Mo K-edge in fluorescence mode at the QAS beam line (7-BM) at NSLS-II. A passivated implanted planar silicon detector (Mirion) was used for the measurements of X-ray fluorescence from the samples. X-ray absorption data were collected by scanning X-ray energy using a Si(111) monochromator across the Mo absorption K-edge (from 200 eV below the edge through 1000 eV above the edge). The spectrum acquisition time was 5 min per scan. Mo foil spectra recorded in reference position simultaneously with the samples were used to align the obtained spectra in X-ray energy. To improve the signal-to-noise ratio, a total of 25 scans were collected and averaged for the a-$MoS_x$ samples. The as-deposited samples were compared to $MoS_2$ and $MoO_3$ reference compounds. EXAFS data processing was performed using Athena and Artemis programs of the Demeter package.[30,31] EXAFS data analysis of Mo K edge spectra was performed by fitting theoretical EXAFS spectra to the experimental data in *r*-space, by applying the Hanning window function to the $k^2$- or $k^3$-weighted data for Fourier transforms (FTs). In the first step, we performed a fit of Mo foil spectra to obtain the value of the amplitude reduction factor, $S_0^2$. A $k^3$-weighting was used in the fit, and the fitting ranges in *k*- and *r*-spaces for Mo foil were 1.3−15.1 and 1.0−3.3 Å, respectively. The obtained value of $S_0^2$ was subsequently fixed in the fits of the experimental EXAFS data of Mo edges in the a-$MoS_x$ films. The fitting model was constructed using crystallographic information of a triangular thiocomplex of molybdenum. Fits of EXAFS signals were performed with $k^3$ weighting in the 2−12(10.5) $Å^{-1}$ *k*-range and 1.2(1.0)−2.71 Å *r*-range for $MoS_6$ ($MoS_4$) AD thin films. Theoretical contribution of Mo/S (Mo/O) photoelectron path(s) was included in the model. Theoretical EXAFS spectra were constructed by using FEFF6.2 code, incorporated in the Artemis program.

## 3. RESULTS AND DISCUSSION

**3.1. $Mo_2S_{12}^{2-}$ Electrochemistry and Film Deposition.** CV scans were carried out on GC substrates in an aqueous electrodeposition bath made of $Mo_2S_{12}^{2-}$ and 0.1 M phosphate buffer solution (pH 7). CV scans, shown in Figure 1, were carried out between 0.1 and −1 V following similar potential cycling experiments reported in the literature.[12,32] We observed a cathodic peak at ∼−0.4 V and an anodic peak at ∼−0.1 V, which we ascribe to the reduction and oxidation of $Mo_2S_{12}^{2-}$, respectively. The cathodic peak noticeably shifts toward more negative potentials during subsequent cycles. AD and CD were carried out at constant potentials of −0.1 and −0.8 V versus Ag/AgCl, respectively (Figure S1); these optimized deposition potentials were selected based on a visual observation of the uniformity of films deposited at different potentials. Films were also deposited by potential cycling between 0.1 and −1 V based on the reports of $MoS_4^{2-}$-based films in the literature.[12,32] Visually, uniform dark brown films were formed on the surface of the FTO substrate regardless of the deposition method used in making the films.

**3.2. a-$MoS_x$ Film Stoichiometry and Characterization.** XPS was used to analyze the products formed in the electrodeposition of the a-$MoS_x$ films. XPS Mo 3p (Figure S2a−c), Mo 3d (Figure S3a−c), and S 2p (Figure 2a−c) region measurements were analyzed for all films, and the peaks in these regions were integrated to determine the S/Mo ratio in a-$MoS_x$ films.

Anodically electrodeposited films made with the $Mo_2S_{12}^{2-}$ precursor afforded a S/Mo ratio of 6.14:1, indicating that a relatively higher S/Mo ratio in the precursor led to sulfur-rich

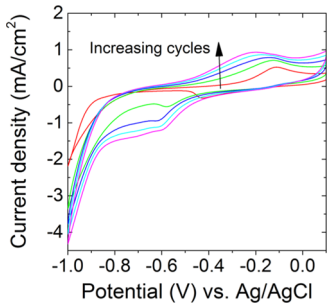


**Figure 1.** CV curves showing the first five CV cycles of 1 mM $Mo_2S_{12}^{2-}$ in a 0.1 M phosphate buffer supporting electrolyte.

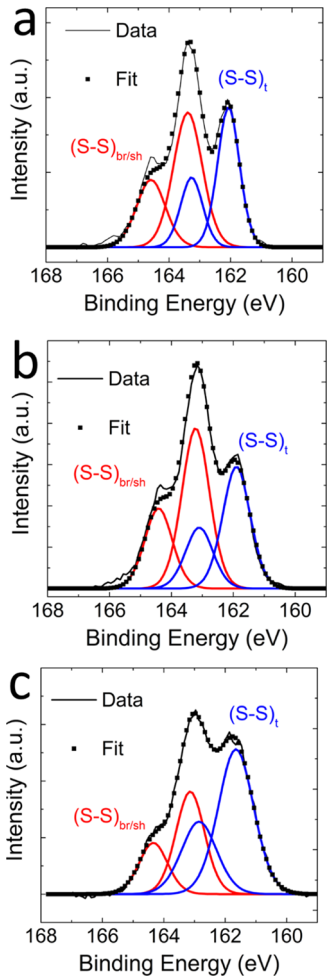


**Figure 2.** XPS S 2p region for (a) AD, (b) CV deposited, and (c) CD samples.



DOI: 10.1021/acsami.9b07277
ACS Appl. Mater. Interfaces 2019, 11, 32879−32886

anodic thin films. This product is consistent with a two-electron oxidation associated with the $Mo_2S_{12}^{2-}$ precursor (1).

$$Mo_2S_{12}^{2-} \rightarrow 2MoS_6 + 2e^- \quad (1)$$

Similarly, anodic oxidation of $MoS_4^{2-}$ precursors on FTO substrates yielded a 4:1 S/Mo (Figure S4a–c) ratio or $MoS_4$ films.

$$MoS_4^{2-} \rightarrow MoS_4 + 2e^- \quad (2)$$

Other studies have reported the formation of $MoS_3$ products from anodic oxidation of $MoS_4^{2-}$ and suggested possible electrochemical oxidation reactions (3).[14]

$$MoS_4^{2-} \rightarrow MoS_3 + 1/8S_8 + 2e^- \quad (3)$$

We speculate that the $MoS_3$ product observed in these experiments is likely a mixture of the two-electron oxidation product (2) and the acidification product (4) formed when the tetrathiomolybdate precursor is dissolved in unbuffered solutions at a pH less than 7.[33,34]

$$MoS_4^{2-} + 2H^+ \rightarrow MoS^3 + H_2S \quad (4)$$

In agreement with eqs 1 and 2, electro-oxidation products of $MoS_4^{2-}$ and $Mo_3S_{13}^{2-}$ have also been reported as $MoS_4$ and $Mo_3S_{13}$, respectively.[21,35] The oxidation product (1) is also in agreement with the reported chemical oxidation of $MoS_4^{2-}$ and $Mo_2S_{12}^{2-}$ anions by chemical oxidants such as iodine, which gave products with a S/Mo ratio of 4 and 6, respectively.

Cathodically electrodeposited films yielded thin films with a S/Mo ratio of 2. The same S/Mo ratio is observed for cathodic films electrodeposited from $MoS_4^{2-}$, suggesting that higher ratios of S/Mo in the thiomolybdate precursor do not affect the stoichiometry of the thin films prepared using CD. Films deposited by potential cycling had a ratio of S/Mo of 4, signifying that these films were a chemical mixture of the cathodic $MoS_2$ and anodic $MoS_6$ products.

Sulfur-rich phases of amorphous metal sulfides have recently generated a great amount of interest as battery materials,[18,19,36] capacitors,[37] and electrocatalysts.[38] $MoS_6$ particles have previously been prepared by chemical oxidation using persulfate or iodine or annealing at low temperatures (240 °C).[19,39,40] To the best of our knowledge, this is the first report of electrodeposited $MoS_6$ thin films. These thin films also have one of the highest known ratios for S/Mo reported in the literature for a-$MoS_x$ materials. The observation that AD leads to a-$MoS_x$ films with the same ratio in the precursor also means sulfur-to-molybdenum ratios as high as 9 could likely be achieved by electrodeposition using $MoS_9^{2-}$ as a precursor.[27]

The sulfur 2p region was analyzed to understand the chemical structure of the electrodeposited samples. All of these samples show two doublets in the S 2p region typical for $Mo_3$ cluster-based metal polysulfides.[41] The lack of a clear peak attributable to elemental sulfur usually observed at higher binding energies compared with the metal polysulfide peaks indicates that most of the sulfur in these films exists as anions which are likely bonded with molybdenum. The first peaks at higher binding energy correspond to shared/bridging ($S_2^{2-}$) and apical ($S^{2-}$) sulfur groups while the second set of peaks belong to terminal ($S_2^{2-}$) sulfides.[21,25]

The ratio of the sulfur peaks at higher binding energies ($S_{HBE}$) to the sulfur peaks at lower binding energies was noticeably larger for AD $MoS_6$ samples than $MoS_2$ samples deposited with cathodic currents, indicating that cathodic samples had a high percentage of sulfur as terminal sulfides while the anodic samples had more bridging/shared sulfides. The $S_{HBE}$ ratios also give us further insight into the difference between anodic samples deposited from $Mo_2S_{12}^{2-}$ precursors and those deposited from $MoS_4^{2-}$ precursors. $MoS_6$ samples made from the sulfur-rich precursor had a higher $S_{HBE}$ ratio than $MoS_4$ samples made from $MoS_4^{2-}$ precursors, indicating that the additional sulfur in these films is incorporated as shared $S_2^{2-}$ moieties.

The local environment and coordination geometry were investigated using EXAFS. These experiments provided evidence that the as-prepared thin films are Mo/S coordination polymers with $Mo_3$ clusters (Figure 3a). The $MoS_6$ thin films

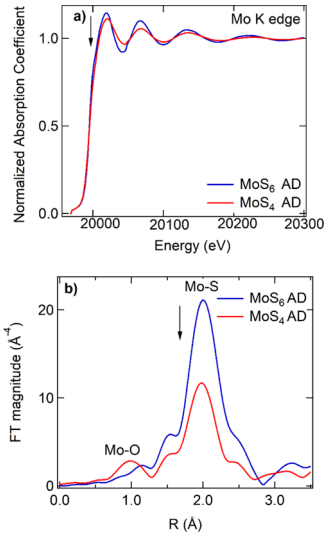


**Figure 3.** (a) Mo K edge X-ray absorption near-edge spectra and (b) FT magnitudes for the a-$MoS_x$ films deposited by AD from the two thiomolybdate precursors that have a ratio of S/Mo (4:1) in $MoS_4$ (red line) and (6:1) in $MoS_6$ (blue line). Arrows indicate the decrease in white line intensity and *r* space intensity.

prepared by the AD method are stable toward surface oxidation as evidenced by the lack of Mo/O species (Figure 3b). A decrease in *r* space intensity is observed in the a-$MoS_4$ film prepared by AD from the $MoS_4^{2-}$ precursor and is directly correlated with the decrease in the coordination of Mo/S pairs (Table S1). Results of EXAFS analysis (Table S1) revealed that both thins films have different Mo/S coordination numbers. The a-$MoS_6$ film prepared using AD from the $Mo_2S_{12}^{2-}$ precursor fitted with a Mo/S scattering path shows a coordination number of 6.3 ± 0.6 closer to the typical seven Mo/S bonds per Mo atom in agreement with previously reported parameters for $Mo_3S_{13}$ clusters with Mo/S (*R* = 2.45 Å),[42] while for a-$MoS_4$, the molybdenum center has a coordination number of 3.8 ± 0.5 consistent with four sulfur ligands. Previous studies have also observed lower Mo/S coordination for electrodeposited thin films of a-$MoS_x$ materials.[42] We hypothesized that the lower coordination number is likely due to oxidation of the $MoS_4$ samples, which was confirmed by EXAFS analysis and the Mo/O species observed from the deconvolution of the XPS Mo 3p region (Figures S4b and S6b). The length of the Mo/S bonds in this material matches well with those in $Mo_3S_{13}$ clusters, and the thin films have no discernible structures beyond the first shell consistent with their amorphous nature (Figure S6).[21,43]



DOI: 10.1021/acsami.9b07277
ACS Appl. Mater. Interfaces 2019, 11, 32879–32886

Raman spectroscopy (Figure 4) and X-ray diffraction (Figure S7) measurements show broad peaks arising from

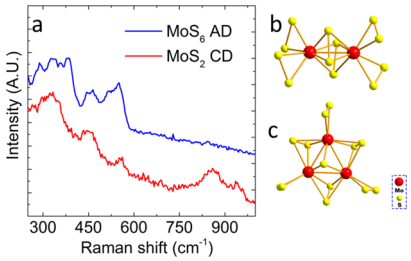


**Figure 4.** (a) Raman spectra for $MoS_6$ samples deposited by anodic currents ($MoS_6$ AD) and $MoS_2$ samples deposited by cathodic currents from a $Mo_2S_{12}^{2-}$ precursor. (b) Structure of $Mo_2S_{12}^{2-}$ precursors and (c) clusters of $Mo_3S_{13}$ in a-$MoS_x$ thin films.

the short-range atomic arrangement present in the inorganic polymeric clusters. Significantly, the broad vibrational bands in the Raman spectra are similar to signature features reported for $Mo_3$ clusters observed for other a-$MoS_x$ materials.[21,44] We observe key differences between cathodic $MoS_2$ and anodic $MoS_6$ thin films. First, the CD samples show broader peaks, suggesting that these samples are less ordered than the AD samples. The Raman spectra of the cathodically grown $MoS_2$ samples show similar peaks but also have peaks at higher wavenumbers corresponding to $Mo^{V}$=O species, showing that these samples are $Mo_3$-based samples that have more defects in the polymers when compared with anodic samples.[21] Other features in the Raman spectra include broad peaks between 280 and 400 $cm^{-1}$ assigned to Mo/S stretching frequencies as previously reported and the peaks between 500 and 550 $cm^{-1}$ associated with the S/S stretching frequencies typical of materials with polysulfide networks.[24,41,44,45] The presence of these peaks suggests that $MoS_6$ and $MoS_2$ samples grown by anodic and cathodic electrochemical deposition are similarly made up of $Mo_3$-like clusters arranged in a coordination inorganic polymer. We hypothesize that the striking similarities between the features prevalent in the $Mo_3$ clusters as examined by Raman spectroscopy to those of the $Mo_2S_{12}$-derived films indicate that the $Mo_2S_{12}^{2-}$ anion in the electrodeposition bath undergoes a structural rearrangement, which affords $Mo_3$ clusters prior to electro-polymerization and deposition on substrates. The lower $S_{HBE}$ ratio of cathodic $MoS_2$ samples shows that these samples are $Mo_3$ clusters with fewer shared sulfide groups compared to anodic $MoS_6$ samples. In agreement with our results, Hibble and Feaviour have observed a similar structural rearrangement of $Mo_2$ clusters to $Mo_3$ clusters after annealing $(NH_4)_2Mo_2S_{12}$ at low temperatures.[46] Structurally, these samples were similar to the $MoS_6$ samples reported herein: sulfur-rich and shown to incorporate more terminal $S_2^{2-}$ moieties, which become shared sulfide groups when the clusters are in a polymer; we hypothesize that our sulfur-rich samples are similarly rich in shared sulfide groups compared to other samples with lower S/Mo ratios.

SEM of $MoS_6$ deposited from $Mo_2S_{12}^{2-}$ precursors for 450 s (Figure 5a) revealed that these films were made up of smaller particles that formed larger aggregates on the order of 100 nm. To gain a better understanding of the morphology and uniformity of the films, we carried out AFM experiments over a 20 $\mu$m × 20 $\mu$m area (Figure 5b). The root-mean-square roughness of this film was relatively small at 5.4 nm, indicating that the $MoS_6$ films were smooth and uniformly deposited on

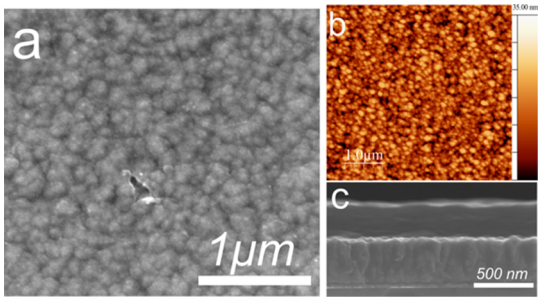


**Figure 5.** (a) SEM images of $MoS_6$ films on FTO substrates, (b) AFM image showing the profile of $MoS_6$ films, and (c) cross-sectional SEM of an ~300 nm $MoS_6$ sample deposited for 400 s.

the FTO substrates. We also visually observed that sulfur-rich thin films grown from $Mo_2S_{12}^{2-}$ precursors were thicker than those grown from $MoS_4^{2-}$ precursors. By comparing the cross-sectional SEM images of $MoS_6$ (Figure 5c) and $MoS_4$ (Figure S8) films grown by anodic electrodeposition from $Mo_2S_{12}^{2-}$ and $MoS_4^{2-}$ for 450 s, respectively, it is seen that the $MoS_6$ films are more than twice as thick as $MoS_4$ films (300 vs 120 nm). The $MoS_6$ and $MoS_4$ films grown for 450 s had mass loadings of 96 ± 4.7 and 62.5 ± 8.3 $\mu g/cm^2$, respectively. Mo loadings of both films can be estimated from the mass loading of molybdenum sulfide and the known stoichiometry of the film and were found to be about 32 $\mu g/cm^2$ for the $MoS_6$ films and 27 $\mu g/cm^2$ for the $MoS_4$ films.

### 3.3. Hydrogen Evolution Catalysis on a-$MoS_x$ Films.

Amorphous (a-$MoS_x$) films deposited on GC substrates were evaluated as hydrogen evolution catalysts in 0.5 M $H_2SO_4$. Linear scanning voltammetry (LSV) scans of a-$MoS_x$ samples deposited from $Mo_2S_{12}^{2-}$ baths using anodic ($MoS_6$), cathodic ($MoS_2$), and CV ($MoS_4$) are shown in Figure 6. The samples

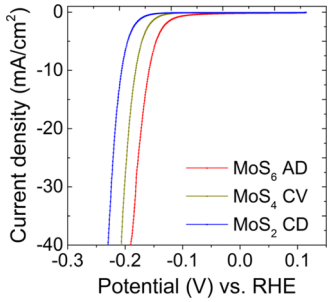


**Figure 6.** HER voltammograms of $MoS_6$, $MoS_4$, and $MoS_2$ films made by anodic, CV, and CD, respectively, in a 0.5 M $H_2SO_4$ electrolyte.

were deposited for different lengths of time and optimized (Figure S9) so that the best catalyst is compared for each sample. Representative LSV curves shown in Figure 6 indicate that $MoS_6$ samples required an overpotential ($\eta_{10}$) of 161 ± 3 mV to achieve a current density of 10 $mA/cm^2$ compared to 182 ± 2 and 212 ± 4 mV for the $MoS_4$ (CV) and $MoS_2$ (CD) samples, respectively (Figure S10). This trend is in agreement with trends reported for a-$MoS_x$ films made from $MoS_4^{2-}$ precursors and suggests that the sulfur content of a-$MoS_x$ films influence their performance as HER catalysts.[47] Yeo also reported higher activity and turnover frequencies for anodic films deposited from $MoS_4^{2-}$ solutions compared to cathodic films from the same precursors.[25] Higher relative sulfur contents were also shown to influence the activity of particle


DOI: 10.1021/acsami.9b07277
ACS Appl. Mater. Interfaces 2019, 11, 32879−32886

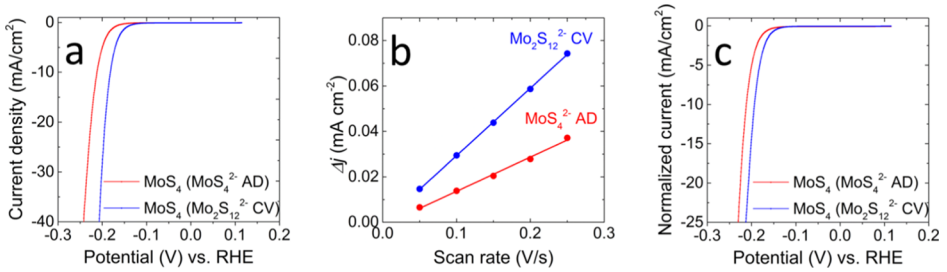


**Figure 7.** (a) LSV scans comparing the hydrogen evolution activity of a $MoS_4$ film grown by AD from $MoS_4^{2-}$ to a $MoS_4$ film grown by CV deposition from $Mo_2S_{12}^{2-}$ precursors. (b) Capacitive currents obtained by CV scans plotted against scan rates are used to compare the relative ECSA of films. (c) LSV scans are normalized by dividing the current densities by the relative ECSA of the films.

samples where the S atoms in $Mo_3S_{13}$ clusters are selectively removed by a low-temperature treatment leading to S/Mo ratios between 2 and 4.[48] The use of $Mo_2S_{12}^{2-}$ precursors allows us to observe trends in the HER activity of a-$MoS_x$ catalysts with ratios of S/Mo higher than 4, and we find that higher sulfur content leads to more active catalysts fully, suggesting that the active sites in a-$MoS_x$ HER catalysts increase with higher sulfur content (up to S/Mo of 6:1).

The ability to independently control the stoichiometry of a-$MoS_x$ thin films using electrochemistry and precursor chemistry also allows decoupling of the influence of the S/Mo ratio and precursor choice on the HER activity of molybdenum sulfides. We compared the HER activity of $MoS_4$ samples made by CV (20 cycles) from $Mo_2S_{12}^{2-}$ to $MoS_4$ films made by using AD (400 s) from $MoS_4^{2-}$ precursors. $MoS_4$ (CV) samples had $\eta_{10}$ overpotentials of 181 mV compared to 210 mV for $MoS_4$ (AD) samples (Figure 7a). To examine the influence of other factors, apart from the effect of stoichiometry on the HER activity of the films, we estimated the electrochemical surface area (ECSA) of both a-$MoS_4$ films in 0.5 M $H_2SO_4$ by measuring the double-layer capacitance ($C_{dl}$) of films using CV at varying scan rates in a potential region with no faradaic currents (Figure S11). The $C_{dl}$ at a chosen potential is then plotted as a function of scan rate as shown in Figure 7b and the slope of this graph gives a quantitative value of the ECSA of the films.[49] $MoS_4$ (CV) films made from $Mo_2S_{12}$ precursors have an ECSA at 0.3 mF/cm$^2$, that is double that for $MoS_4$ (AD) deposited for 400 s. Similar experiments were carried out for $MoS_6$ films (Figure S12). When currents are normalized by the measured (Figure 7c) ECSA (i.e., by dividing the currents of $MoS_4$ (CV) films by 2), the difference in $\eta_{10}$ between the films is reduced to only 10 mV, indicating that the S/Mo ratio of a-$MoS_x$ films and their surface areas play a significant role in their measured HER activities.

### 3.4. Long-Term Tests and Post-HER Characterization.

Long-term tests for the most active sample, the AD $MoS_6$, were carried out by voltammetry by taking an LSV scan and comparing it to another LSV taken after 1000 CV cycles between 0.2 and −0.2 V versus RHE. These scans (Figure 8a) show a slight degradation of the HER activity of films with the $\eta_{10}$ overpotential increasing from 159 to 165 mV. We carried out a second long-term test by holding a constant current of 10 mA/cm$^2$ over 10 000 s (Figure 8b). We find that the potential required to maintain this current density increases from 159 to 181 mV during this period. This degradative loss can be attributed to the decrease of active sites through a process in which terminal sulfide groups are gradually substituted by water.[25,50]

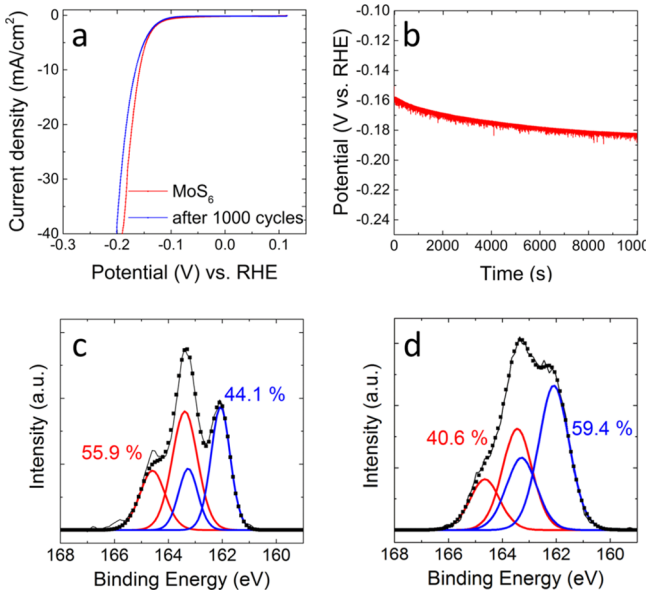


**Figure 8.** Stability tests for $MoS_6$ film showing (a) linear voltammetry scans before and after 1000 CVs between 0.2 and −0.25 V. (b) Constant current density of 10 mA/cm$^2$ for 10 000 s. XPS S 2p region $MoS_6$ films (c) before and (d) after long-term tests.

In agreement with these reports, we also observed a decrease in the S/Mo ratio from 6 to 4.25 by XPS in the S 2p region after long-term constant current tests. Additionally, the ratio of the sulfur peaks at higher binding energies ($S_{HBE}$) to the sulfur peaks at lower binding energies for the $MoS_6$ sample decreased from ∼56 to 41% after long-term tests, indicating a decrease in the relative amount of shared sulfide moieties and an increase in the relative amount of terminal sulfide moieties in the samples (Figure 8c,d). Post-electrochemical characterization by XPS gives us a clear picture of the activity and deactivation of the catalysts that were AD as a-$MoS_6$. The results indicate that sulfur-rich a-$MoS_6$ films are initially polymeric $Mo_3$ clusters made up of more shared sulfide moieties than samples less rich in sulfur. These shared sulfide moieties serve as active sites for the HER but are activated and converted to terminal sulfide moieties in a process that can be described as a "depolymerization" process. In related work, researchers have suggested that these terminal sulfides are likely to be gradually replaced by water ligands leading to a slow deactivation of $MoS_6$ catalysts.[50]

## 4. CONCLUSIONS

In conclusion, we have synthesized and characterized electrodeposited a-$MoS_x$ samples from $Mo_2S_{12}^{2-}$ deposition baths.


DOI: 10.1021/acsami.9b07277
ACS Appl. Mater. Interfaces 2019, 11, 32879−32886

Our results show that cathodic and anodic samples have a S/Mo ratio of 2 and 6, respectively. The anodic $MoS_6$ films also have one of the highest known values for the ratio of S/Mo reported in the literature for a-$MoS_x$ materials. Our results indicate that the stoichiometry of the precursor is maintained in anodic samples while cathodic samples show a S/Mo ratio of 2 regardless of the relative amount of S in the precursor. The $MoS_6$ film, like other a-$MoS_x$ materials, is a polymer of $Mo_3$ clusters with the additional S atoms existing as shared sulfide groups. We show that the activity of a-$MoS_x$ films depend on the relative amount of sulfur in these films and their ECSAs. By taking advantage of the ability to control stoichiometry via electrochemistry and precursor of choice, we were able to systematically control and improve the electrochemical activity of these films as HER catalysts. Characterization of the films after long-term tests reveal that these additional sulfur atoms in S-rich films are gradually depleted through a depolymerization process in which the shared sulfide groups are converted to terminal sulfide moieties and are replaced by water ligands.

## ■ ASSOCIATED CONTENT

### Supporting Information

The Supporting Information is available free of charge on the ACS Publications website at DOI: 10.1021/acsami.9b07277.

a-$MoS_x$ deposition plots, additional XPS spectra, LSV scans, and ECSA plots (PDF)

## ■ AUTHOR INFORMATION


### Corresponding Author

*E-mail: mullins@che.utexas.edu.

### ORCID

Yang Liu: 0000-0002-7240-1546

Anatoly I. Frenkel: 0000-0002-5451-1207

C. Buddie Mullins: 0000-0003-1030-4801


### Notes

The authors declare no competing financial interest.

## ■ ACKNOWLEDGMENTS

The authors gratefully acknowledge the National Science Foundation for grant no. CHE-1664941 and the Welch Foundation for grant F-1436. O.M. gratefully acknowledges a National Science Foundation (NSF) Integrative Graduate Education and Research Traineeship (IGERT) grant 0966298 for financial support. They also acknowledge the National Science Foundation (grant 0618242) for funding the X-ray photoelectron spectrometer used in this work. A.I.F. acknowledges the support of the U.S. DOE grant no. DE-FG02-03ER15476 for the X-ray absorption spectroscopy measurements and analysis part of this research. This research used beam line 7-BM (QAS) of the National Synchrotron Light Source II, a U.S. DOE Office of Science User Facility operated for the DOE Office of Science by Brookhaven National Laboratory under contract no. DE-SC0012704. Beam line operations were supported in part by the Synchrotron Catalysis Consortium (U.S. DOE, Office of Basic Energy Sciences, grant no. DE-SC0012335).

## ■ REFERENCES


(1) Bard, A. J.; Fox, M. A. Artificial Photosynthesis: Solar Splitting of Water to Hydrogen and Oxygen Water Splitting. *Acc. Chem. Res.* **1995**, *28*, 141−145.

(2) Lewis, N. S.; Nocera, D. G. Powering the Planet: Chemical Challenges in Solar Energy Utilization. *Proc. Natl. Acad. Sci. U.S.A.* **2006**, *103*, 15729−15735.

(3) Nocera, D. G. Personalized Energy: The Home as a Solar Power Station and Solar Gas Station. *ChemSusChem* **2009**, *2*, 387−390.

(4) Bard, A. J. Inner-Sphere Heterogeneous Electrode Reactions. Electrocatalysis and Photocatalysis: The Challenge. *J. Am. Chem. Soc.* **2010**, *132*, 7559−7567.

(5) Vesborg, P. C. K.; Seger, B.; Chorkendorff, I. Recent Development in Hydrogen Evolution Reaction Catalysts and Their Practical Implementation. *J. Phys. Chem. Lett.* **2015**, *6*, 951−957.

(6) Feng, L.; Vrubel, H.; Bensimon, M.; Hu, X. Easily-prepared dinickel phosphide ($Ni_2P$) nanoparticles as an efficient and robust electrocatalyst for hydrogen evolution. *Phys. Chem. Chem. Phys.* **2014**, *16*, 5917−5921.

(7) Popczun, E. J.; McKone, J. R.; Read, C. G.; Biacchi, A. J.; Wiltrout, A. M.; Lewis, N. S.; Schaak, R. E. Nanostructured Nickel Phosphide as an Electrocatalyst for the Hydrogen Evolution Reaction. *J. Am. Chem. Soc.* **2013**, *135*, 9267−9270.

(8) Hinnemann, B.; Moses, P. G.; Bonde, J.; Jørgensen, K. P.; Nielsen, J. H.; Horch, S.; Chorkendorff, I.; Nørskov, J. K. Biomimetic Hydrogen Evolution: $MoS_2$ Nanoparticles as Catalyst for Hydrogen Evolution. *J. Am. Chem. Soc.* **2005**, *127*, 5308−5309.

(9) Jaramillo, T. F.; Jorgensen, K. P.; Bonde, J.; Nielsen, J. H.; Horch, S.; Chorkendorff, I. Identification of Active Edge Sites for Electrochemical $H_2$ Evolution from $MoS_2$ Nanocatalysts. *Science* **2007**, *317*, 100−102.

(10) Kibsgaard, J.; Chen, Z.; Reinecke, B. N.; Jaramillo, T. F. Engineering the surface structure of $MoS_2$ to preferentially expose active edge sites for electrocatalysis. *Nat. Mater.* **2012**, *11*, 963−969.

(11) Wang, H.; Lu, Z.; Xu, S.; Kong, D.; Cha, J. J.; Zheng, G.; Hsu, P.-C.; Yan, K.; Bradshaw, D.; Prinz, F. B.; Cui, Y. Electrochemical tuning of vertically aligned $MoS_2$ nanofilms and its application in improving hydrogen evolution reaction. *Proc. Natl. Acad. Sci. U.S.A.* **2013**, *110*, 19701−19706.

(12) Merki, D.; Fierro, S.; Vrubel, H.; Hu, X. Amorphous Molybdenum Sulfide Films as Catalysts for Electrochemical Hydrogen Production in Water. *Chem. Sci.* **2011**, *2*, 1262−1267.

(13) Merki, D.; Hu, X. Recent Developments of Molybdenum and Tungsten Sulfides as Hydrogen Evolution Catalysts. *Energy Environ. Sci.* **2011**, *4*, 3878−3888.

(14) Morales-Guio, C. G.; Hu, X. Amorphous Molybdenum Sulfides as Hydrogen Evolution Catalysts. *Acc. Chem. Res.* **2014**, *47*, 2671−2681.

(15) Vrubel, H.; Moehl, T.; Grätzel, M.; Hu, X. Revealing and Accelerating Slow Electron Transport in Amorphous Molybdenum Sulphide Particles for Hydrogen Evolution Reaction. *Chem. Commun.* **2013**, *49*, 8985−8987.

(16) Benck, J. D.; Chen, Z.; Kuritzky, L. Y.; Forman, A. J.; Jaramillo, T. F. Amorphous Molybdenum Sulfide Catalysts for Electrochemical Hydrogen Production: Insights into the Origin of Their Catalytic Activity. *ACS Catal.* **2012**, *2*, 1916−1923.

(17) Tang, M. L.; Grauer, D. C.; Lassalle-Kaiser, B.; Yachandra, V. K.; Amirav, L.; Long, J. R.; Yano, J.; Alivisatos, A. P. Structural and Electronic Study of an Amorphous MoS3 Hydrogen-Generation Catalyst on a Quantum-Controlled Photosensitizer. *Angew. Chem.* **2011**, *123*, 10385−10389.

(18) Doan-Nguyen, V. V. T.; Subrahmanyam, K. S.; Butala, M. M.; Gerbec, J. A.; Islam, S. M.; Kanipe, K. N.; Wilson, C. E.; Balasubramanian, M.; Wiaderek, K. M.; Borkiewicz, O. J.; Chapman, K. W.; Chupas, P. J.; Moskovits, M.; Dunn, B. S.; Kanatzidis, M. G.; Seshadri, R. Molybdenum Polysulfide Chalcogels as High-Capacity, Anion-Redox-Driven Electrode Materials for Li-Ion Batteries. *Chem. Mater.* **2016**, *28*, 8357−8365.

(19) Wang, X.; Du, K.; Wang, C.; Ma, L.; Zhao, B.; Yang, J.; Li, M.; Zhang, X.-X.; Xue, M.; Chen, J. Unique Reversible Conversion-Type Mechanism Enhanced Cathode Performance in Amorphous Molybdenum Polysulfide. *ACS Appl. Mater. Interfaces* **2017**, *9*, 38606−38611.

(20) Ye, H.; Ma, L.; Zhou, Y.; Wang, L.; Han, N.; Zhao, F.; Deng, J.; Wu, T.; Li, Y.; Lu, J. Amorphous $MoS_3$ as the sulfur-equivalent cathode material for room-temperature Li−S and Na−S batteries. *Proc. Natl. Acad. Sci. U.S.A.* **2017**, *114*, 13091−13096.
(21) Tran, P. D.; Tran, T. V.; Orio, M.; Torelli, S.; Truong, Q. D.; Nayuki, K.; Sasaki, Y.; Chiam, S. Y.; Yi, R.; Honma, I.; Barber, J.; Artero, V. Coordination Polymer Structure and Revisited Hydrogen Evolution Catalytic Mechanism for Amorphous Molybdenum Sulfide. *Nat. Mater.* **2016**, *15*, 640−646.
(22) Staszak-Jirkovský, J.; Malliakas, C. D.; Lopes, P. P.; Danilovic, N.; Kota, S. S.; Chang, K.-C.; Genorio, B.; Strmcnik, D.; Stamenkovic, V. R.; Kanatzidis, M. G.; Markovic, N. M. Design of active and stable Co−Mo−$S_x$ chalcogels as pH-universal catalysts for the hydrogen evolution reaction. *Nat. Mater.* **2016**, *15*, 197−203.
(23) Truong, Q. D.; Kempaiah Devaraju, M.; Nguyen, D. N.; Gambe, Y.; Nayuki, K.; Sasaki, Y.; Tran, P. D.; Honma, I. Disulfide-Bridged ($Mo_3S_{11}$) Cluster Polymer: Molecular Dynamics and Application as Electrode Material for a Rechargeable Magnesium Battery. *Nano Lett.* **2016**, *16*, 5829−5835.
(24) Nguyen, D. N.; Nguyen, L. N.; Nguyen, P. D.; Thu, T. V.; Nguyen, A. D.; Tran, P. D. Crystallization of Amorphous Molybdenum Sulfide Induced by Electron or Laser Beam and Its Effect on $H_2$-Evolving Activities. *J. Phys. Chem. C* **2016**, *120*, 28789−28794.
(25) Ting, L. R. L.; Deng, Y.; Ma, L.; Zhang, Y.-J.; Peterson, A. A.; Yeo, B. S. Catalytic Activities of Sulfur Atoms in Amorphous Molybdenum Sulfide for the Electrochemical Hydrogen Evolution Reaction. *ACS Catal.* **2016**, *6*, 861−867.
(26) Deng, Y.; Ting, L. R. L.; Neo, P. H. L.; Zhang, Y.-J.; Peterson, A. A.; Yeo, B. S. Operando Raman Spectroscopy of Amorphous Molybdenum Sulfide ($MoS_x$) during the Electrochemical Hydrogen Evolution Reaction: Identification of Sulfur Atoms as Catalytically Active Sites for $H^+$ Reduction. *ACS Catal.* **2016**, *6*, 7790−7798.
(27) Draganjac, M.; Simhon, E.; Chan, L. T.; Kanatzidis, M.; Baenziger, N. C.; Coucouvanis, D. Synthesis, Interconversions, and Structural Characterization of the Molybdenum Sulfide Anions, $[(S_4)_2MoS]^{2-}$, $[(S_4)_2MoO]^{2-}$, $(Mo_2S_{10})^{2-}$ and $(Mo_2S_{12})^{2-}$. *Inorg. Chem.* **1982**, *21*, 3321−3332.
(28) Daage, M.; Chianelli, R. R. Structure-Function Relations in Molybdenum Sulfide Catalysts: The "Rim-Edge" Model. *J. Catal.* **1994**, *149*, 414−427.
(29) Huang, Z.; Luo, W.; Ma, L.; Yu, M.; Ren, X.; He, M.; Polen, S.; Click, K.; Garrett, B.; Lu, J.; Amine, K.; Hadad, C.; Chen, W.; Asthagiri, A.; Wu, Y. Dimeric $[Mo_2S12]^{2-}$ Cluster: A Molecular Analogue of $MoS_2$ Edges for Superior Hydrogen-Evolution Electrocatalysis. *Angew. Chem.* **2015**, *127*, 15396−15400.
(30) Ravel, B.; Newville, M. ATHENA, ARTEMIS, HEPHAESTUS: data analysis for X-ray absorption spectroscopy usingIFEFFIT. *J. Synchrotron Radiat.* **2005**, *12*, 537−541.
(31) Newville, M. IFEFFIT : interactive XAFS analysis andFEFFfitting. *J. Synchrotron Radiat.* **2001**, *8*, 322−324.
(32) Merki, D.; Vrubel, H.; Rovelli, L.; Fierro, S.; Hu, X. Fe, Co, and Ni Ions Promote the Catalytic Activity of Amorphous Molybdenum Sulfide Films for Hydrogen Evolution. *Chem. Sci.* **2012**, *3*, 2515−2525.
(33) Afanasiev, P. Synthetic Approaches to the Molybdenum Sulfide Materials. *C. R. Chim.* **2008**, *11*, 159−182.
(34) Lin, T.-W.; Liu, C.-J.; Lin, J.-Y. Facile synthesis of $MoS_3$/carbon nanotube nanocomposite with high catalytic activity toward hydrogen evolution reaction. *Appl. Catal., B* **2013**, *134−135*, 75−82.
(35) Du, K.; Zheng, L.; Wang, T.; Zhuo, J.; Zhu, Z.; Shao, Y.; Li, M. Electrodeposited $Mo_3S_{13}$ Films from $(NH_4)_2Mo_3S_{13}\cdot 2H_2O$ for Electrocatalysis of Hydrogen Evolution Reaction. *ACS Appl. Mater. Interfaces* **2017**, *9*, 18675−18681.
(36) Sakuda, A.; Ohara, K.; Fukuda, K.; Nakanishi, K.; Kawaguchi, T.; Arai, H.; Uchimoto, Y.; Ohta, T.; Matsubara, E.; Ogumi, Z.; Okumura, T.; Kobayashi, H.; Kageyama, H.; Shikano, M.; Sakaebe, H.; Takeuchi, T. Amorphous Metal Polysulfides: Electrode Materials with Unique Insertion/Extraction Reactions. *J. Am. Chem. Soc.* **2017**, *139*, 8796−8799.
(37) Jiang, Z.; Lu, W.; Li, Z.; Ho, K. H.; Li, X.; Jiao, X.; Chen, D. Synthesis of Amorphous Cobalt Sulfide Polyhedral Nanocages for High Performance Supercapacitors. *J. Mater. Chem. A* **2014**, *2*, 8603−8606.
(38) Wang, C.; Wang, T.; Liu, J.; Zhou, Y.; Yu, D.; Cheng, J.-K.; Han, F.; Li, Q.; Chen, J.; Huang, Y. Facile Synthesis of Silk-Cocoon S-Rich Cobalt Polysulfide as an Efficient Catalyst for the Hydrogen Evolution Reaction. *Energy Environ. Sci.* **2018**, *11*, 2467−2475.
(39) Afanasiev, P.; Bezverkhy, I. Synthesis of $MoS_x(5 > x > 6)$ Amorphous Sulfides and Their Use for Preparation of $MoS_2$ Monodispersed Microspheres. *Chem. Mater.* **2002**, *14*, 2826−2830.
(40) Afanasiev, P.; Jobic, H.; Lorentz, C.; Leverd, P.; Mastubayashi, N.; Piccolo, L.; Vrinat, M. Low-Temperature Hydrogen Interaction with Amorphous Molybdenum Sulfides $MoS_x$. *J. Phys. Chem. C* **2009**, *113*, 4139−4146.
(41) Hellstern, T. R.; Kibsgaard, J.; Tsai, C.; Palm, D. W.; King, L. A.; Abild-Pedersen, F.; Jaramillo, T. F. Investigating Catalyst-Support Interactions To Improve the Hydrogen Evolution Reaction Activity of Thiomolybdate $[Mo_3S_{13}]^{2-}$ Nanoclusters. *ACS Catal.* **2017**, *7*, 7126−7130.
(42) Lassalle-Kaiser, B.; Merki, D.; Vrubel, H.; Gul, S.; Yachandra, V. K.; Hu, X.; Yano, J. Evidence from in Situ X-Ray Absorption Spectroscopy for the Involvement of Terminal Disulfide in the Reduction of Protons by an Amorphous Molybdenum Sulfide Electrocatalyst. *J. Am. Chem. Soc.* **2015**, *137*, 314−321.
(43) Yadgarov, L.; Rosentsveig, R.; Leitus, G.; Albu-Yaron, A.; Moshkovich, A.; Perfilyev, V.; Vasic, R.; Frenkel, A. I.; Enyashin, A. N.; Seifert, G.; Rapoport, L.; Tenne, R. Controlled Doping of $MS_2$ (M = W, Mo) Nanotubes and Fullerene-like Nanoparticles. *Angew. Chem., Int. Ed.* **2012**, *51*, 1148−1151.
(44) Kibsgaard, J.; Jaramillo, T. F.; Besenbacher, F. Building an appropriate active-site motif into a hydrogen-evolution catalyst with thiomolybdate $[Mo_3S_{13}]^{2-}$ clusters. *Nat. Chem.* **2014**, *6*, 248−253.
(45) Chang, C.; Chan, S. S. Infrared and Raman studies of amorphous $MoS_3$ and poorly crystalline $MoS_2$. *J. Catal.* **1981**, *72*, 139−148.
(46) Hibble, S. J.; Feaviour, M. R. An in situ structural study of the thermal decomposition reactions of the ammonium thiomolybdates, $(NH_4)_2Mo_2S_{12}\cdot 2H_2O$ and $(NH_4)_2Mo_3S_{13}\cdot 2H_2O$. *J. Mater. Chem.* **2001**, *11*, 2607−2614.
(47) Vrubel, H.; Hu, X. Growth and Activation of an Amorphous Molybdenum Sulfide Hydrogen Evolving Catalyst. *ACS Catal.* **2013**, *3*, 2002−2011.
(48) Lee, C.-H.; Lee, S.; Lee, Y.-K.; Jung, Y. C.; Ko, Y.-I.; Lee, D. C.; Joh, H.-I. Understanding the Origin of Formation and Active Sites for Thiomolybdate $[Mo_3S_{13}]^{2-}$ Clusters as Hydrogen Evolution Catalyst through the Selective Control of Sulfur Atoms. *ACS Catal.* **2018**, *8*, 5221−5227.
(49) McCrory, C. C. L.; Jung, S.; Ferrer, I. M.; Chatman, S. M.; Peters, J. C.; Jaramillo, T. F. Benchmarking Hydrogen Evolving Reaction and Oxygen Evolving Reaction Electrocatalysts for Solar Water Splitting Devices. *J. Am. Chem. Soc.* **2015**, *137*, 4347−4357.
(50) Dave, M.; Rajagopal, A.; Damm-Ruttensperger, M.; Schwarz, B.; Nägele, F.; Daccache, L.; Fantauzzi, D.; Jacob, T.; Streb, C. Understanding Homogeneous Hydrogen Evolution Reactivity and Deactivation Pathways of Molecular Molybdenum Sulfide Catalysts. *Sustainable Energy Fuels* **2018**, *2*, 1020−1026.


DOI: 10.1021/acsami.9b07277
*ACS Appl. Mater. Interfaces* 2019, 11, 32879−32886